IEEE Access
Multidisciplinary | Rapid Review | Open Access Journal

Received October 28, 2020, accepted November 13, 2020, date of publication November 17, 2020,
date of current version December 1, 2020.

Digital Object Identifier 10.1109/ACCESS.2020.3038637

Quantitative Monitoring of Geological Hazards With CORS Network Data and Load Impact Change: A Case Study in Zhejiang, China

PENGFEI XU[1,2], AIQIN LI[3], CHUANYIN ZHANG[2], YANG LIU[1,2], AND WANQIU LI[4]

[1]College of Geomatics, Shandong University of Science and Technology, Qingdao 266590, China
[2]Chinese Academy of Surveying & Mapping, Beijing 100830, China
[3]ZJ Academy of Surveying & Mapping, Hangzhou 310012, China
[4]School of Surveying and Geo-Informatics, Shandong Jianzhu University, Jinan 250101, China

Corresponding author: Chuanyin Zhang (zhangchy@casm.ac.cn)

This work was supported in part by the National Natural Science Foundation of China under Grant 41674024, in part by the Basic Scientific Research Operating Expenses of the Chinese Academy of Surveying and Mapping under Grant 7771806 and Grant AR1905, and in part by the Innovation Program for Postgraduates of Shandong University of Science and Technology under Grant SDKDYC190203.

ABSTRACT Geological hazard monitoring plays a pivotal role in preventing geological hazards. The main challenge faced by many experiments is to quantitatively monitor and analyze geological hazards. This paper proposes a quantitative monitoring indicator, called the ground surface stability anomaly (GSSA), for the first time and gives the identification criterion of the GSSA based on three stability factors. The features of the three stability factors, including geodetic height, ground gravity, and vertical deviation, reflect the relationship between load-induced changes and geological hazards. To verify the effectiveness and applicability of the GSSA quantitative monitoring method, a regional GSSA model was constructed based on the continuously operating reference station (CORS) network data and load impact data in southeastern Zhejiang, China. The larger the value of the GSSA is, the more likely geological hazards are to occur, especially when an abnormal dynamic environment (such as heavy rainfall, sea level anomaly, atmospheric pressure anomaly, or spring tide) is encountered. By comparing the GSSA with the potential trouble points of geological hazards and 40 geological hazard events that have occurred, the results show that the method can quantitatively, accurately, and continuously monitor the GSSA in an area covered by the CORS network, and the method has the ability to capture the precursors to geological hazards.

INDEX TERMS Ground surface stability anomaly, CORS network, load impact, geological hazard monitoring, GNSS.

I. INTRODUCTION

Geological hazard monitoring has received considerable critical attention, and it plays a pivotal role in preventing geological hazards. Geological hazards occur frequently in southeastern Zhejiang, China, which mainly include debris flows, landslides, and collapses. Geological hazards threaten the local living environment, life and property, which is why geological hazard monitoring has become more significant in this area [1].

The main task of geological hazard monitoring is to obtain information on the process of geological hazards in time and space, including deformation, geophysical and geochemical fields, groundwater and predisposing factors [2]–[5]. Much work has thus far focused on deformation monitoring, which has become one of the main bases for geological hazard prevention [6]–[8]. Interferometric synthetic aperture radar (InSAR), remote-sensing sensors, global navigation satellite systems (GNSS), geodetic surveying, and terrestrial laser scanning technologies are all conventional methods of deformation monitoring [9]–[14]. Stress monitoring, earth pulsation measurements, geochemical methods and geoacoustic monitoring are commonly used for monitoring geophysical and geochemical fields [15]–[18]. The common methods of groundwater monitoring are the measurement of groundwater level (or groundwater pressure), pore water pressure and groundwater quality. Heavy precipitation and engineering activity, monitored by meteorological means, are the main

The associate editor coordinating the review of this manuscript and approving it for publication was Halil Ersin Soken.

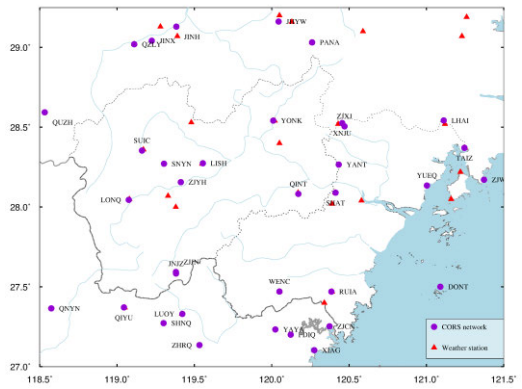

FIGURE 1. **The distribution of CORS and weather stations in southeastern Zhejiang.**

predisposing factors of geological hazards [3], [7], [19]–[24]. The predisposing factors including heavy rainfall, sea level anomaly, atmospheric pressure anomaly, and spring tide, are called abnormal dynamic environments in this paper.

Despite its long success, geological hazard monitoring has many problems in practice. InSAR and remote sensing are usually used to monitor slow-moving landslides, but they are not efficient in monitoring faster and more catastrophic events. Continuous regional-scale monitoring has been largely underexplored, and too little work has been devoted to it [25]–[27]. Continuously operating reference station (CORS) ground-fixed observation stations continuously observe satellite navigation signals for a long period of time to obtain observation data and transmit the observation data to the data center in real time or at regular intervals through a communication facility [3]. Several studies have revealed that the CORS network can continuously obtain the dynamic positioning information of fixed stations in the area as a spatial reference for dynamic monitoring, and provide sufficient data support for continuous regional-scale monitoring [28]–[30]. However, the key problem of geological disaster monitoring is the lack of an effective quantitative indicator to monitor and analyze geological disasters. Quantitative monitoring and early warning systems are limited by a large amount of background information and the complexity of geological hazards [31]–[39].

This study proposes a new quantitative monitoring method for ground surface stability anomalies (GSSAs). To realize continuous regional-scale monitoring of geological hazards, the geodetic height, the ground gravity and the vertical deviation have been introduced as stability factors, which reflect the relationship between load-induced changes and geological hazards. The present study was designed to determine GSSA quantitative indicators based on the relationship between the load impact of the three stability factors and geological disasters. It is worth mentioning that this method refers to regional-scale monitoring and analysis rather than analysis of on one specific site. It is a 'top-down' approach as defined by Cascini(2008), and contributes a novel insight to the quantitative monitoring of geological hazards [40].

To verify the validity of the method, a regional GSSA model was constructed based on the Zhejiang CORS network data from January 2015 to December 2017 in southeastern Zhejiang, China. By comparing the GSSA with the potential danger points of geological hazards and 40 geological hazard events that have occurred, the reliability of this method can be tested.

II. METHODS

A. LOAD DEFORMATION THEORY

Changes in the ground environment lead to changes in load and thus to changes in stability factors [3], [41], [42].The surface environmental load changes mainly include the load impact caused by changes in the atmosphere, soil moisture, sea level and groundwater [42]–[46]. Load change can be illustrated by equivalent water height (EWH) [41], [42], [47]–[49]. Based on the load deformation theory, the normalized load spherical harmonic expansion is:

$$\Delta h_v(\varphi,\lambda) = R\sum_{i=1}^{L}\sum_{m=0}^{l} \times\left[\Delta C_{lm}^{q}\cos m\lambda + \Delta S_{im}^{q}\sin m\lambda\right]\bar{P}_{lm}(\sin\varphi) \quad (1)$$

where (φ,λ) represents the geocentric latitude and longitude of the ground calculation point, while C_{lm}^{q}, ΔS_{lm}^{q} is the normalized load sphere harmonic coefficient with degree l and order $m \cdot \bar{P}_{l\,\mathrm{m}}(*)$. l is the fully normalized associated Legendre function with degree m and order.

Each load change can be expressed by EWH. The changes in the position of the ground station or the changes in ground gravity caused by EWH change can be expressed by the load Green's function integral method [3], [41], [42], [47].

$$\Delta\theta(\varphi,\lambda) = \mathrm{G}\rho_{\mathrm{v}}\iint_{S}\frac{\Delta h_w\left(\varphi',\lambda'\right)}{n}G(\psi)\mathrm{dS} \quad (2)$$

where $\left(\varphi',\lambda'\right)$ is the ground flow point; G is the gravitational constant; n is the spatial distance from the flow point to the calculation point; S is the surface area of the earth; $\rho_w \approx 10^3\ kg\cdot m^{-3}$ represents the density of water; $\mathrm{G}(\psi)$ is the general load Green's function; and ψ is the spherical angular distance.

Based on the theory of load spherical harmonic coefficients, the load changes of the surface environment can also be calculated by the spherical harmonic coefficients.

The changes in geodetic height can be calculated by:

$$\varepsilon(\varphi,\lambda) = 3\frac{\rho_x}{\rho_e}\frac{GM}{\gamma R}\sum_{i=2}^{L}\frac{h_l'}{2l+1} \cdot\sum_{m=0}^{l}\left[\Delta C_{lm}^{q}\cos m\lambda + \Delta S_{i\ln}^{q}\sin m\lambda\right]\bar{P}_{\ln}(\sin\varphi) \quad (3)$$

The changes in ground gravity can be calculated by:

$$g_t(\varphi,\lambda) = -3\frac{\rho_w}{\rho_e}\frac{GM}{R^2}\sum_{l=2}^{L}\frac{l+2\,h_l'-(l+1)\mathrm{k}_l'}{2l+1} \cdot\sum_{m-0}^{l}\left[\Delta C_{lm}^{q}\cos m\lambda + \Delta S_{lm}^{q}\sin m\lambda\right]\bar{P}_{lm}(\sin\varphi) \quad (4)$$

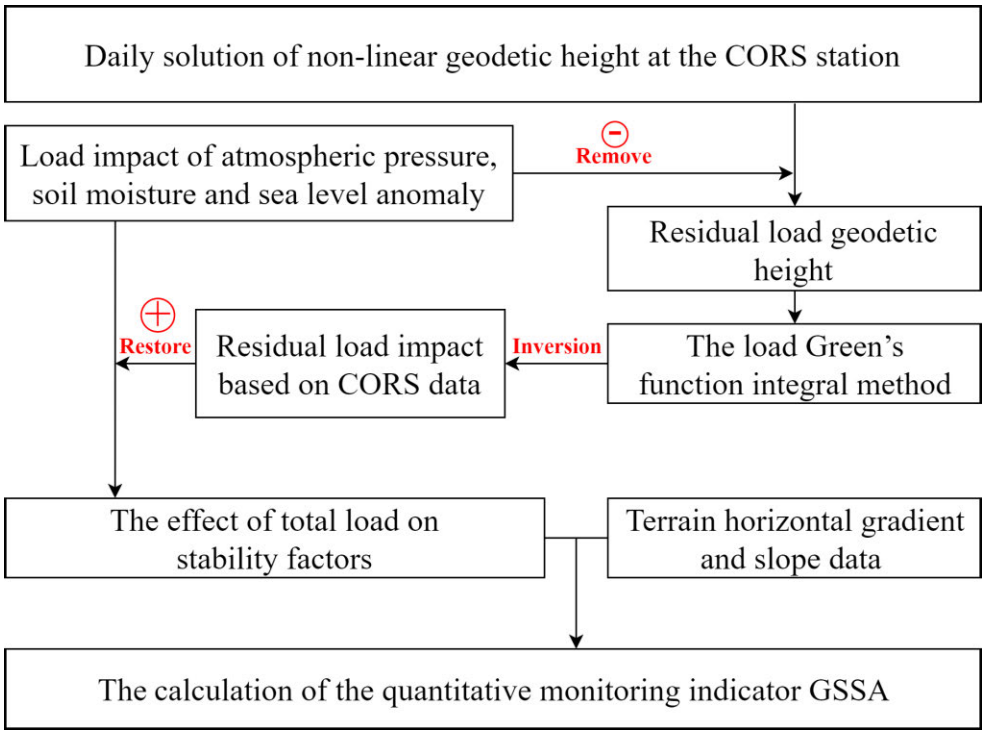

FIGURE 2. A schematic diagram of the solutions of the quantitative monitoring indicator GSSA.

The changes in vertical deviation can be calculated by:

$$\begin{aligned}&\text{southing}: \zeta^s \\ &= \frac{GM}{\gamma r^2}\sin\varphi \sum_{i=2}^{L}\left(1+k_l'-h_l'\right)\left(\frac{R}{r}\right)^{'} \\ &\quad\cdot \sum_{m-0}^{'}\left[\Delta C_{lm}^{q}\cos m\lambda+\Delta S_{lm}^{q}\sin m\lambda\right]\frac{\partial}{\partial\theta}\bar{P}_{lm}(\sin\varphi) \\ &\text{westing}: \eta^s \\ &= \frac{GM}{\gamma r^2\sin\varphi}\sum_{l-2}^{L}\left(1+k_l'-h_l'\right)\left(\frac{R}{r}\right)^{'} \\ &\quad\cdot \sum_{m=1}^{l} m\left[\Delta C_{lm}^{q}\cos m\lambda+\Delta S_{lm}^{q}\sin m\lambda\right]\bar{P}_{lm}(\sin\varphi)\end{aligned} \tag{5}$$

In Eqs. (3)-(5), k_l' is the load Love number; h_l' is the radial load Love number; R $\rho_e \approx 5.5\times10^3$ kg $\cdot$ m^{-3} calculates the average density of the solid earth; M is the mass of the earth; R is the average radius of the earth; r illustrates the distance from the calculation point to the earth's core, and γ is the average gravity on the ground.

According to Eq. (2), the changes in nonlinear ground height at the CORS station can be expressed as:

$$\Delta r = \mathrm{G}\rho_w \iint_S \frac{\Delta h_w\left(\varphi',\lambda\right)}{n} G(\psi)'\mathrm{dS}+\varepsilon \tag{6}$$

where $G(\psi)^r$ is the radial load Green's function and ε is the nonload vertical deformation (vertical tectonic deformation and vertical deformation of the groundwater balance). The daily solution of ground height can be calculated using CORS network data. Due to the abundant rainfall in the study area, the effect of groundwater balance is not obvious, and vertical tectonic deformation is very small, so this paper treats it as random noise [42].

Eq. (6) is used directly to invert the load impact caused by changes in the regional surface environment (atmosphere, soil moisture, river, lake, and groundwater changes). However, due to the complexity of the surface environment, the inversion stability and the accuracy of the results are low. As shown in Figure2, the load impact of atmospheric pressure, soil moisture and sea level can be calculated by using Eqs. (3) to (5). Then, the three load impacts are removed from the changes in the nonlinear geodetic height of the CORS station to obtain the changes in the residual load geodetic height (this step can be called 'remove'). The inversion results of the residual load equivalent water height can be solved by using Eq. (6). The residual load impact can be achieved according to the load Green's function integral method. It should be pointed out that residual load impact is mainly caused by the influence of groundwater. Finally, we add the three load impacts and the residual load impact to obtain the total load impact (this step can be called 'restore'). The total load is the surface environmental load mentioned above. The accuracy and stability of load influence inversion results based on CORS network data can be improved by 'remove' and 'restore' technology [20], [41], [48], [50].

B. QUANTITATIVE SOLUTIONS OF GSSA

Using the above methods, this study obtained the load deformation field model in the study area. The method that quantitatively calculates the GSSA will be further explained below.

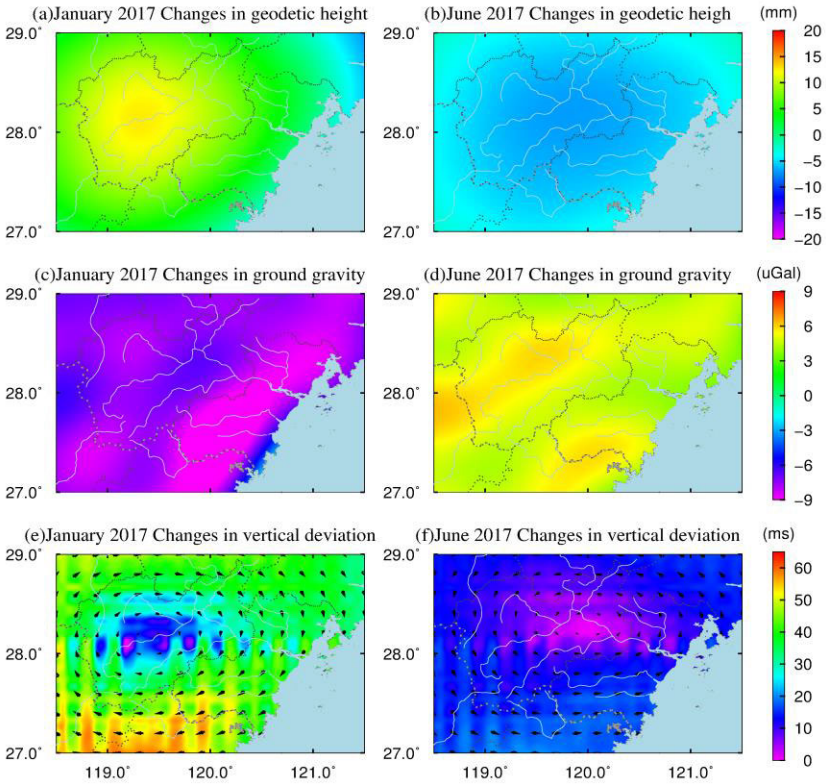

FIGURE 3. The total load impact of three stability factors in southeastern Zhejiang.

The geodetic height, ground gravity and vertical deviation are all important variables for geological hazard monitoring, and they are distinctive both in the temporal dimension and all spatial dimensions in regard to the sensitivity of the GSSA. The changes in ground gravity are so sensitive in the temporal dimension that it helps to quickly capture the signal of GSSA. However, because its functioning range tends to be inversely proportional to the square of distance, the spatial range of the changes is hard to recognize. In comparison, geodetic height is less influenced by distance since it is only inversely proportional to distance, so it tends to be more sensitive in regard to the spatial range but less sensitive in the temporal dimension. Since these two variables are isotropic, vertical deviation is introduced, which can obtain GSSA information in different directions, not to mention its sensitivity to far-zone effects. In this paper, the three variables are called stability factors [3], [41], [51].

According to the relationship between the three stability factors and geological disasters, the quantitative identification criteria of GSSAs are proposed, as shown in Table 1. Criterion 1 in which there are changes in geodetic height and ground gravity, points to the uplift of the ground; criterion 2 leads to local uneven deformation of the ground. Criterion 1, concerning the vertical deviation, the results in the surrounding ground being stretched; criterion 2 creates an extra tractive force along the slope direction. Meanwhile, criterion 3 mainly considers the impact of slope on the GSSA. Obviously, any of the above phenomena will lead to an increase in the risk of geological hazards and the value of the GSSA according to Eq. (7). Terrain horizontal gradient and slope data were calculated based on CORS network data. Then, the computational formula of the GSSA can be developed from the criterion illustrated below:

$$\begin{aligned} GSSA_{\varepsilon,g,s} &= \operatorname{sgn}(A_{\varepsilon,g,s}) \left|A_{\varepsilon,g,s}\right|^{n_a} Q_a \\ &\quad + \operatorname{sgn}(B_{\varepsilon,g,s}) \left|B_{\varepsilon,g,s}\right|^{n_b} Q_b + \operatorname{sgn}(C) \left|C\right|^{n_c} Q_c \\ A_{\varepsilon,g,s} &= (a_{\varepsilon,g,s} - \bar{a}_{\varepsilon,g,s})/\sigma_a \\ B_{\varepsilon,g,s} &= (b_{\varepsilon,g,s} - \bar{b}_{\varepsilon,g,s})/\sigma_b \\ C_{\varepsilon,g,s} &= (c - \bar{c})/\sigma_c \\ Q_* &= \frac{q_*}{q_a + q_b + q_c} \end{aligned} \tag{7}$$

$GSSA_{\varepsilon,g,s}$ in Eq. (7), respectively represents the GSSA of geodetic height, ground gravity and vertical deviation; $a_{\varepsilon,g,s}$ shows, respectively, the rate of the variation in geodetic height, ground gravity and vertical deviation, while $b_{\varepsilon,g,s}$ is the horizontal gradient of geodetic height and ground gravity and the vector inner product of rate of change and horizontal gradient, respectively. c is the value of the slope while $\bar{a}_{\varepsilon,g,s}$, $\bar{b}_{\varepsilon,g,s}$ and $\bar{c}$ are the averages within certain time series. σ_a, σ_b and σ_c are the corresponding standard deviations, and n_a, n_b and n_c accordingly represent the exponential parameters; q_a, q_b and q_c are, respectively, the weight of a, b and c; sgn(*)

TABLE 1. The identification criterion of GSSAs.

Stability factors	Identification criterion①	Identification criterion②	Identification criterion③
Geodetic height	The rate of change increasing (more than zero)	The horizontal gradient growing larger	The terrain slope increasing
Ground gravity	The rate of change decreasing (less than zero)	The horizontal gradient growing larger	The effect of disturbed gravity on topography increasing
Vertical deviation	The vertical deviation diverging	The vector inner product of rate of change and horizontal gradient growing larger	The terrain slope increasing

is the sign function, which is related to the identification criteria in Table 1. It must be mentioned that $GSSA_{\varepsilon,g,s}$ is a dimensionless variable without units.

III. DATA

This study takes the southeastern area of Zhejiang Province (118.5° E-121.5°E, 27°N-29°N) as the study site, and mainly relies on Zhejiang CORS network data, weather station measured data and global model observation data of atmospheric pressure, soil water and sea-level anomalies (the changes in rivers, lakes and reservoirs in this paper have been omitted).

A. ATMOSPHERIC LOAD

The global atmospheric pressure model was downloaded from the European Centre for Medium-Range Weather Forecasts (ECMWF), and has a monthly resolution of $0.5°\times0.5°$. As shown in Figure 2, weather station data were downloaded from the National Meteorological Information Center (NMIC), and covers 46 stations along the study area, where a regional atmospheric pressure model was obtained. The monthly atmospheric load deformation field changes, with a resolution of $1'\times1'$ were solved by using the load deformation theory and removal and restoration technology in southeastern Zhejiang [41].

B. SOIL MOISTURE LOAD

The Noah ground surface model from the Global Land Data Assimilation System (GLDAS) mainly includes 0-200 cm of land surface soil water, plant canopy surface water, and snow water changes, with a monthly resolution of $0.25°\times0.25°$. The 360-degree spherical harmonic coefficient was calculated by Eq. (1) based on the equivalent water height of soil moisture. The spherical harmonic coefficients were used to obtain the monthly soil moisture load deformation field with a resolution of $1'\times1'$ by Eqs. (3) to (5) [46].

C. SEA LEVEL LOAD

The sea level anomaly data were accessed from Archiving, Validation, and Interpretation of Satellites Oceanographic (AVISO) data and are presented as Maps of Sea Level Anomaly (MSLA), with a monthly resolution ratio of $0.25°\times0.25°$. With the elimination of the impact of steric sea level, the sea level anomaly caused by mass can be assured [44]. The calculation process of the monthly $1'\times1'$ sea level load deformation field is the same as above [45].

D. RESIDUAL LOAD

The Zhejiang CORS network has been providing centimeter-scale data in the province since 2008. As shown in Figure 2, this paper selected the data of 38 CORSs along the southeastern coast from January 2015 to December 2017. The monthly mean value of geodetic height changes was achieved based on the data of 38 CORSs (the geocentric motion and polar motion were removed). The load impact of the atmosphere, soil moisture and river and sea level anomalies were removed, and then the $1'\times1'$ inversion results of the residual load were solved by Eq. (6). It should be pointed out that residual load impact is mainly caused by the influence of groundwater [3], [41].

E. TOTAL LOAD

The monthly $1'\times1'$ total load deformation field was calculated by adding the residual load deformation field and the load deformation field of the atmosphere, soil moisture and sea level load [3]. The statistical results are shown in Table 2.

IV. RESULTS AND ANALYSIS

A. THE RESULTS OF THE RELATIVE GSSA

According to Eq. (7), the results of the total load impact of three stability factors were used to construct the relative GSSA model by setting the weights of the rate of change, horizontal gradient and terrain slope, which takes the

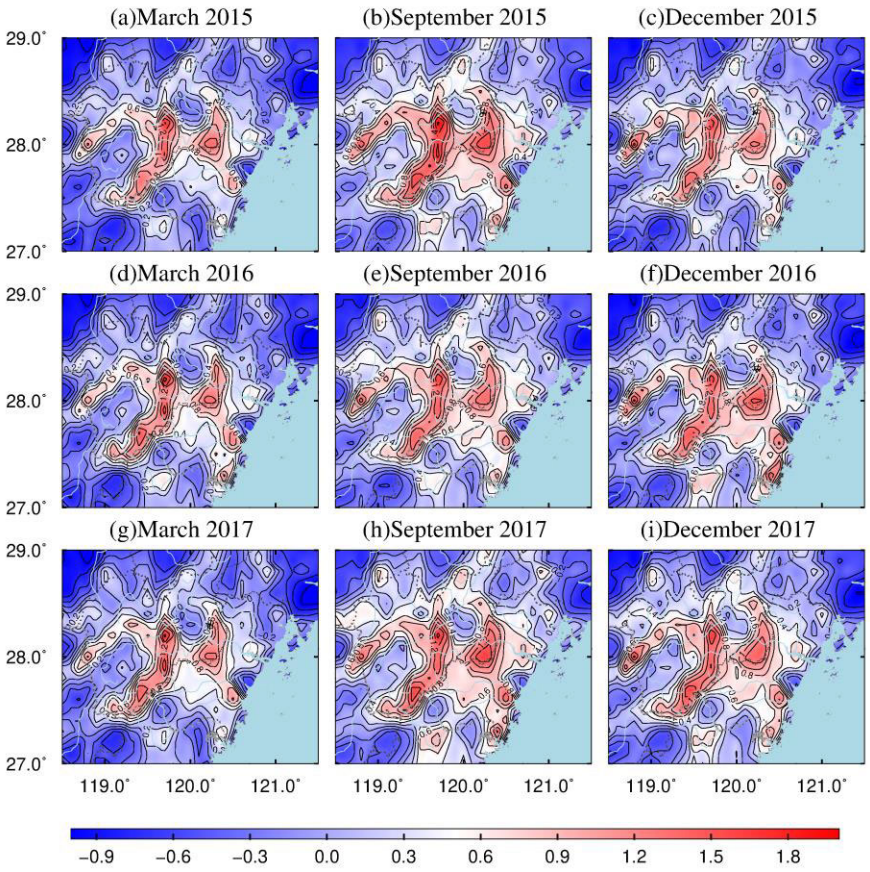

FIGURE 4. The relative GSSA in southeastern Zhejiang.

TABLE 2. Effect of total load on stability factors in southeastern Zhejiang from 2015 to 2017.

Stability factors	Max.	Min.	Ave.	Rms.	Annual variation
Geodetic height(mm)	16.71	-31.96	-4.06	8.91	40.18
Ground gravity(uGal)	12.64	-10.78	-0.52	4.68	17.96
Vertical deviation(ms)	66.79	-57.44	-1.54	16.18	79.68

*The annual variation is the difference between the maximum and minimum values in a year.

consistency of geological hazardous events and the relative GSSA as the optimization criterion. After data processing by the normalization method, the time series of the relative GSSA is obtained from January 2015 to December 2017.

The relative GSSA indicates the changes in the value of the GSSA from the last month, reflecting the real-time dynamic and spatial differences in the GSSA. For example, if the relative GSSA value of the current month is greater than zero, it means that the stability of the ground has decreased compared with the last month, and the possibility of geological hazards has increased. As shown in Figure 4, the red part shows that the value of the relative GSSA is large and the stability of this location is decreasing.

B. THE RESULTS OF THE GSSA

Using the time series of the relative GSSA, after processing by the accumulation operation and removing the mean, the GSSA regional model was constructed. The benchmark of GSSA results is the average of January 2015 to December 2017.Compared with the relative GSSA, the GSSA results suggest the cumulative effect of the time domain and the difference in distinctive locations at the same time.

As far as the GSSA is concerned, a large value indicates that at this time, the stability is low, and a rising value means a decrease in stability. In detail, (1) within the relative GSSA (Figure 4), a larger value indicates that the stability of the ground is decreasing, and when the value starts to increase, the decrease in stability is intensified. (2) Regarding the GSSA (Figure 5), a large value indicates that the stability of the ground is low, and an increasing value means that the stability is decreasing.

C. MONITORING AND ANALYSIS OF GEOLOGICAL HAZARDS

To test the practicability and reliability of the GSSA quantitative monitoring method, this study compared the difference in

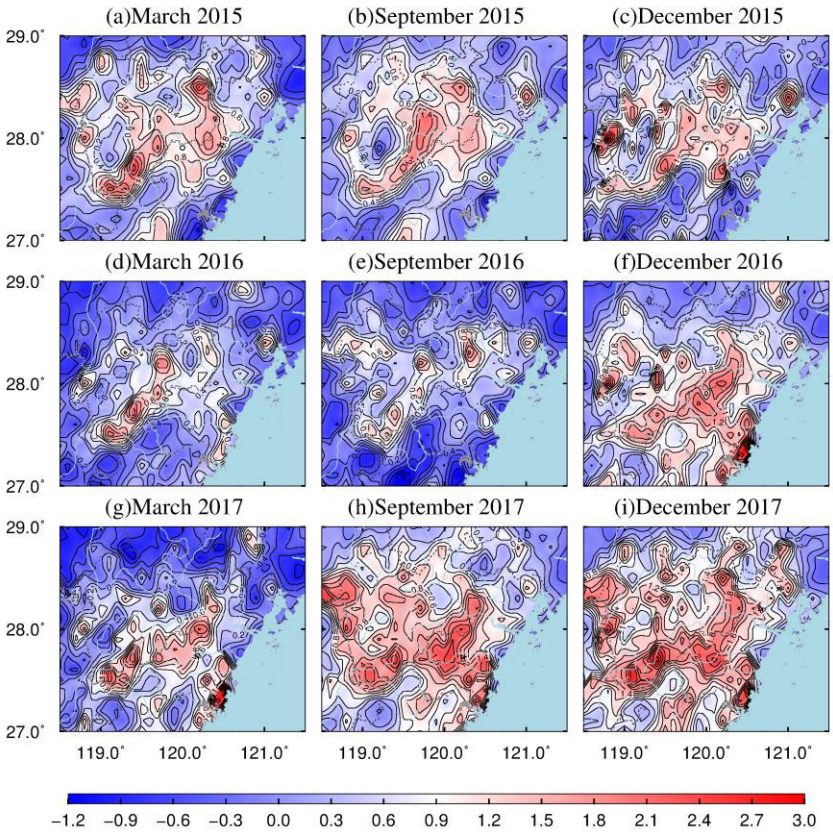

FIGURE 5. The GSSA in southeastern Zhejiang.

the spatial distribution of the overall GSSA with the potential geological hazard trouble sites. The data of potential hazardous sites can be obtained from the geological hazard prevention plan of Zhejiang Province. As shown in Figure 6 (the data of hazardous sites in some districts were not obtained, so the figure only shows those with valid data), the blue area with a small value indicates that the ground stability of the location is good, and it can be considered that the ground nearby is generally stable. In contrast, the ground stability is poor in the red area. It is obvious that the potentially hazardous sites are mainly located in the red area, and their distribution has a strong consistency with the distribution of areas with large GSSA values. Therefore, the GSSA quantitative indicators can effectively reflect the difference in ground stability in a CORS-covered area and provide a significant reference basis for the discovery of new potential hazardous sites.

To analyze the relationship among the quantitative monitoring indicator GSSA and abnormal dynamics of the environment and geological hazards, this study collected data from news networks and government reports for forty hazardous events that occurred during the time range from January 2015 to December 2017. Figure 7 (a) and (b) show that on August 21st, 2015, there was a debris flow in Wencheng County. From June 2015 until the time when the hazard occurred, the relative GSSA and GSSA values in this place continued to increase, reflecting a decreasing ground stability at a gradually accelerated speed. The point in the time series where the minimum of the relative GSSA and the GSSA appears is referred to in this paper as the precursor of geological hazards. It is obvious that the precursor was captured fifty days ahead of the geological hazard. This hazard was accompanied by heavy rainfall, and the lowest atmospheric pressure led to the bulging of the ground and thus the decrease of its stability in Figure 7 (c). Therefore, heavy rainfall and low atmospheric pressure are the main predisposing factors of this geological hazard. On October 10th, 2016, there was a collapse in Qintian. According to the time series of the relative GSSA and the GSSA, the precursor occurred ninety days ahead of the event. When the collapse occurred, in addition to heavy rainfall and low atmospheric pressure, the sea level value was regionally at a maximum in Figure 7 (d). Therefore, the vertical deviation leaned towards the sea and lowered the stability of the sea side of the mountain. The precursor of the Taishun debris flow that occurred on August 2nd, 2017, was captured eighty days ahead of the debris flow. Heavy rainfall occurred just one day before the hazard, and the sea level anomaly was at its minimum rather than its maximum. It is worth noting that when the sea level value was at its minimum, the load caused by the sea level anomaly decreased, and

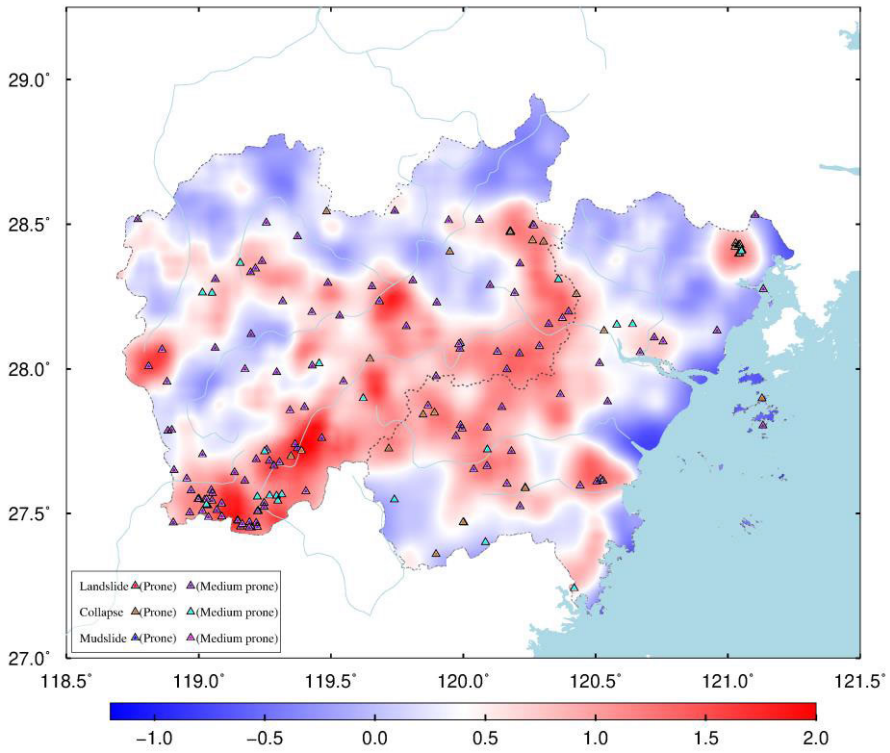

FIGURE 6. The overall GSSA and potential hazardous sites in southeastern Zhejiang.

the ground bounced back up, so the stability also diminished. None of the spring tides were monitored during the three hazards, but the occurrence of spring tides would lead to the bulging of the ground and a decrease in gravity, which could also cause geological hazards. Based on the analysis above, the precursors to forty geological hazards captured by GSSA quantitative monitoring methods and abnormal dynamics of the environment are illustrated in detail in Table 3.

Super Typhoon Soudelor (International Number 1513) landed on the Zhejiang coast on August 8th, 2015 and influenced the study area to a great extent. Of the forty hazardous events collected, six occurred on August 8th and 9th, as shown in Table 3. Figure 7 (c) shows that the heaviest rain occurred in 2015 and a sharp decrease in atmospheric pressure occurred at the time of the geological hazard. The heavy rainfall and lowering of the atmospheric pressure caused by the super typhoon constituted the main predisposing factors of the regional geological hazards. Similarly, the Super Typhoon Megi (International Number 1617) on December 28th, 2016, resulted in low atmospheric pressure and the heaviest rain of the year, which caused five of the geological hazards of the forty hazardous events collected. Based on the analysis above, the GSSA quantitative monitoring method is demonstrated to be effective in capturing and obtaining the precursors to geological hazards.

Therefore, in practical applications, a GSSA quantitative monitoring of geological hazards can be carried out in the following steps. First, CORS network observations are used to calculate the effect of regional total load on three stability factors. Then, we combine the regional total load impact and the data of the horizontal gradient and terrain slope and use Eq. (7) to construct the regional model of GSSA quantitative monitoring. We consider past geological hazards as prior information. Following the principle that geological hazards agree with the GSSA model, the best GSSA regional model can be obtained by gradually adjusting the ratio of the stability factors. Finally, based on the two features of GSSA quantitative monitoring (the minimum of the relative GSSA and the GSSA time series), we constantly trace and monitor the abnormal dynamics of the environment after the precursor appears. Thus, regional geological hazards would be monitored and prevented.

V. DISCUSSION

Normally, the increase in rainfall would correspond with the decrease in atmospheric pressure. As shown in Table 3, atmospheric pressure and rainfall are the two major predisposing factors concerning geological hazards in the study area, while tide height tends to be less influential. However, this conclusion could have been limited by the quality of observation data since atmospheric pressure and rainfall are data measured daily by weather stations, while tide height and sea level change are data measured monthly by global models, so the resolution ratio and accuracy of the latter two are not guaranteed. As far as the two features of geological disaster precursors based on the GSSA above are concerned,

TABLE 3. The results of geological hazard precursors and abnormal dynamic environments.

	Types of geological hazards	Time (year/month/day)	Quantitative monitoring			Abnormal dynamic environment			
			①	②	Days ahead	③	④	⑤	⑥
1	Debris Flow	2015/07/10	√	√	5	√	√	∪	×
2	Debris Flow	2015/08/01	√	√	30	×	×	+	√
3	Landslide	2015/08/08	√	√	45	√	√	+	×
4	Debris Flow	2015/08/08	√	√	30	√	√	+	×
5	Debris Flow	2015/08/08	√	√	45	√	√	+	×
6	Collapse	2015/08/08	√	√	40	√	√	+	×
7	Debris Flow	2015/08/08	√	√	35	√	√	+	×
8	Landslide	2015/08/09	√	√	35	√	√	+	×
9	Landslide	2015/08/14	√	√	45	×	×	+	√
10	Landslide	2015/08/19	√	√	50	√	×	+	×
11	Debris Flow	2015/08/21	√	√	50	√	√	+	×
12	Landslide	2015/11/13	√	√	30	√	√	∩	√
13	Landslide	2015/11/16	√	×	45	√	√	∩	×
14	Landslide	2016/01/23	√	√	80	×	√	-	√
15	Landslide	2016/01/30	×	×	/	×	√	∪	×
16	Landslide	2016/04/23	√	√	120	√	√	+	√
17	Landslide	2016/05/08	×	√	30	×	√	-	√
18	Landslide	2016/05/27	×	√	10	√	×	∪	×
19	Landslide	2016/05/29	√	√	15	√	√	∪	×
20	Debris Flow	2016/08/09	√	√	50	√	×	+	×
21	Debris Flow	2016/08/09	×	√	45	√	×	+	×
22	Collapse	2016/08/09	×	×	/	√	×	+	×
23	Landslide	2016/09/15	√	√	50	√	√	∩	√
24	Debris Flow	2016/09/15	√	√	120	√	√	∩	√
25	Landslide	2016/09/15	√	√	60	√	√	∩	√
26	Debris Flow	2016/09/19	√	√	80	×	×	∩	×
27	Landslide	2016/09/21	√	√	50	×	×	∩	×
28	Collapse	2016/09/21	√	√	70	×	×	∩	×
29	Landslide	2016/09/28	√	√	15	√	√	∩	√
30	Landslide	2016/09/28	√	√	75	√	√	∩	√
31	Debris Flow	2016/09/28	√	√	150	√	√	∩	√
32	Landslide	2016/09/28	√	√	60	√	√	∩	√
33	Landslide	2016/09/28	√	√	60	√	√	∩	√
34	Landslide	2016/10/08	√	√	40	×	×	∩	×
35	Collapse	2016/10/10	√	√	90	√	√	∩	×
36	Collapse	2017/02/02	√	√	70	×	×	∪	√
37	Collapse	2017/04/03	×	√	45	×	×	-	√
38	Collapse	2017/07/03	√	×	60	√	×	+	×
39	Landslide	2017/08/02	√	√	80	√	√	+	×
40	Collapse	2017/11/27	√	×	100	×	×	∪	×

①: Precursor captured by the relative GSSA; ②: Precursor captured by the GSSA; ③: Reduced atmospheric pressure; ④: Increased rainfall; ⑤: Sea level anomaly; ⑥ Spring tide

√: Representation has this feature; +: Increase; -: Decrease; ∩: Maximum; ∪: Minimum

when both arise, the GSSA quantitative monitoring method has a 'strong' ability to capture the precursors; when only one arises, the ability is 'weak'; if neither appears, the capturing can be announced as a failure. As shown in Table 4, the GSSA quantitative monitoring method performs well in regard to debris flows, with a 'strong' evaluation of 91% cases, but not

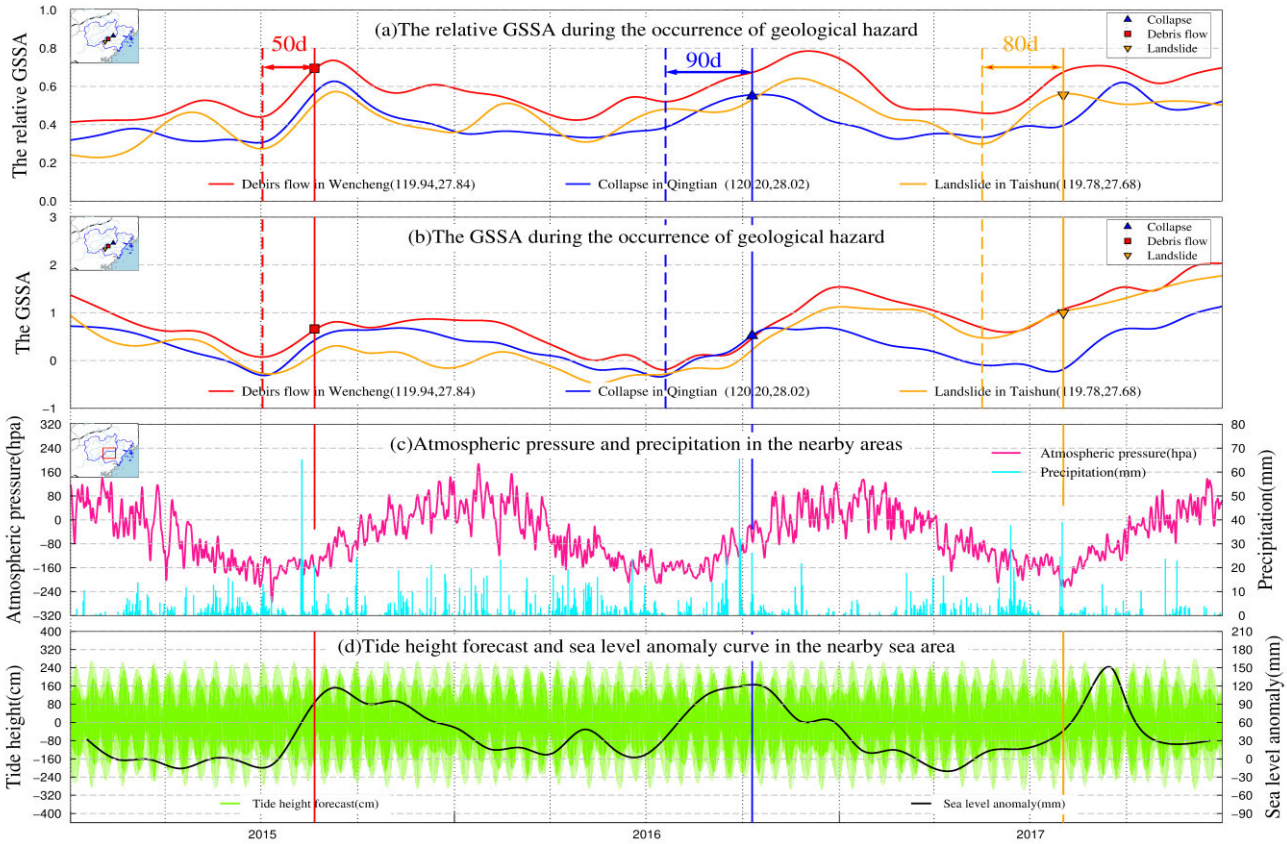

FIGURE 7. Illustration of the precursors to geological hazards and abnormal dynamic environments.

TABLE 4. The performance statistics of the approach to capturing precursors.

Type of hazard	Strong ability	Weak ability	Fail to capture	Average days ahead
Landslide	16	4	1	33
Debris flow	10	1	0	58
Collapse	4	3	1	67

very well in capturing collapses. In 75% percent of the 40 geological hazards, the relative GSSA and the GSSA simultaneously captured the precursors, and the cases where they both failed accounted for 5% of the geological hazards. The causes for geological hazards are complex, and the events in which capturing of precursors failed might have been caused by artificial engineering or other nonenvironmental factors. This concept is beyond the scope of this study. As illustrated in Table 4, the precursors to landslides are usually captured 33 days beforehand, while debris flows and collapses are captured approximately two months beforehand. The statistical results function as a significant reference to the application of the method and the analysis of geological hazards.

It must be noted that the capture of geological hazard precursors does not achieve prediction, but it could help to recognize areas that are fragile to hazards and arrange monitoring and alerts. In practical applications, we are supposed to issue alerts at the time when abnormal dynamic environmental factors are observed, not when there appears to be a precursor. After the occurrence of geological hazard precursors, if abnormal environmental dynamics appear, geological hazards are likely to take place. However, without obvious abnormal dynamics, disasters still might occur. Abnormal dynamic environments are predisposing factors of geological hazards but are not necessary. In summary, this study demonstrated the ability of the GSSA quantitative monitoring method to capture the precursors to geological hazards. The method also analyzed the relationships among the GSSA, abnormal dynamics of the environment and geological hazards. There are also deficiencies: Eq. (7) still needs definite agreement to resolve the weight; the impact ratio of the three stability factors on the GSSA requires more experiments and tests. The calculation of the GSSA is expected to rise in accuracy and efficiency if the method is to be combined with machine learning in the next phase of the study. It is obvious that any single technique is not able to deal with every problem. The GSSA quantitative monitoring method generates the ability to capture hazard precursors, and if it is integrated with other

observing approaches (InSAR, GNSS, level, ground gravity, etc.), especially with the existing monitoring and alerting systems, an increase in the early warning ability can be expected.

VI. CONCLUSION

Based on the relationship between the effect of total load on the three stability factors and geological disasters, this paper proposes a new quantitative monitoring indicator GSSA for the first time, and nine quantitative identification criteria(in Table 1) are constructed to calculate the GSSA using CORS network data. Southeastern Zhejiang is taken as a target area to test and analyze the practicability and effectiveness of the GSSA quantitative monitoring method.

The method works well in aspects such as regional-scale monitoring, continuous monitoring and quantitative monitoring. Through a comparison of the spatial distribution of the total GSSA with potential hazardous points, this approach is able to accurately reveal the differences in ground stability. The focused monitoring of unstable districts provides significant references to the discovery of new potential points. After the monitoring and analysis of forty hazards, the relation among the quantitative monitoring indicator GSSA, the abnormal dynamics of environment and geological hazards was expounded, and two super typhoons were discovered as the main predisposing factors of many geological hazards in particular. The results suggest that the GSSA quantitative monitoring method is capable of capturing precursors of geological disasters. In practical applications, the method can effectively identify areas with poor or decreasing ground stability. Combined with the observation of abnormal dynamics of the environment, it can accomplish the constant quantitative monitoring and analysis of relative hazards. The method is presented as a novel insight and approach for quantitative monitoring of regional geological hazards, and it has both great significance and reference value to the construction of an early warning model based on past hazardous events.

REFERENCES

[1] X. M. Tang, H. J. Feng, T. H. Ma, W. Li, and J. Chang, "Issue of forecast and early-warning information on burst geological hazards in Zhejiang Province based on ArcIMS technology," *Chin. J. Geological Hazard Control*, vol. 18, no. 2, pp. 117–121, Feb. 2007.

[2] G. Q. Wang, B. Yan, W. J. Gan, J. H. Geng, G.-R. Xiao, and J. Shen, "NChina16: A stable geodetic reference frame for geological hazard studies in North China," *J. Geodyn.*, vol. 115, pp. 10–22, Jan. 2018.

[3] W. Wang, C. Zhang, M. Hu, Q. Yang, S. Liang, and S. Kang, "Monitoring and analysis of geological hazards in three gorges area based on load impact change," *Natural Hazards*, vol. 97, no. 2, pp. 611–622, Jul. 2019.

[4] F. Cotecchia, F. Santaloia, P. Lollino, C. Vitone, G. Pedone, and O. Bottiglieri, "From a phenomenological to a geomechanical approach to landslide hazard analysis," *Eur. J. Environ. Civil Eng.*, vol. 20, no. 9, pp. 1004–1031, Oct. 2014.

[5] L. Cascini, C. Cascini, J. Corominas, R. Jibson, and J. MonteroOlarte, "Landslide hazard and risk zoning for urban planning and development," in *Proc. Int. Conf. Landslide Risk Manage.*, London, U.K.: Taylor and Francis, Jan. 2005, pp. 199–235.

[6] M. Fall, R. Azzam, and C. Noubactep, "A multi-method approach to study the stability of natural slopes and landslide susceptibility mapping," *Eng. Geol.*, vol. 82, no. 4, pp. 241–263, Feb. 2006.

[7] R. Fell, J. Corominas, C. Bonnard, L. Cascini, E. Leroi, and W. Z. Savage, "Guidelines for landslide susceptibility, hazard and risk zoning for land use planning," *Eng. Geol.*, vol. 102, nos. 3–4, pp. 85–98, Dec. 2008.

[8] C. Huang, H. Xia, and J. Hu, "Surface deformation monitoring in coal mine area based on PSI," *IEEE Access*, vol. 7, pp. 29672–29678, 2019.

[9] F. Cigna, B. Osmanoğlu, E. Cabral-Cano, T. H. Dixon, J. A. Ávila-Olivera, V. H. Garduño-Monroy, C. DeMets, and S. Wdowinski, "Monitoring land subsidence and its induced geological hazard with synthetic aperture radar interferometry: A case study in Morelia, Mexico," *Remote Sens. Environ.*, vol. 117, pp. 146–161, Feb. 2012.

[10] A. B. Huang, C. C. Wang, J. T. Lee, and Y. T. Ho, "Applications of FBG-based sensors to ground surface stability monitoring," *J. Rock Mech. Geotech. Eng.*, vol. 8, no. 04, pp. 513–520, Aug. 2016.

[11] D. Liverman, M. Batterson, D. Taylor, and J. Ryan, "Geological hazards and disasters in newfoundland and Labrador," *Can. Geotechnical J.*, vol. 38, no. 5, pp. 936–956, Oct. 2001.

[12] M. Wang, Z. K. Sheng, and D. N. Dong, "Effects of non-tectonic crustal deformation on continuous GPS position time series and correction to them," *Chin. J. Geophys.*, vol. 48, no. 5, pp. 1045–1052, May 2005.

[13] R. Huang and W. Li, "Development and distribution of Geohazards triggered by the 5.12 Wenchuan Earthquake in China," *Sci. China Ser. E, Technol. Sci.*, vol. 52, no. 4, pp. 810–819, Mar. 2009.

[14] F. Guzzetti, A. Carrara, M. Cardinali, and P. Reichenbach, "Landslide hazard evaluation: A review of current techniques and their application in a multi-scale study, central italy," *Geomorphology*, vol. 31, nos. 1–4, pp. 181–216, Dec. 1999.

[15] Z. Y. Han and X. Q. Xue, "Status and development trend of monitoring technology for geological hazards," *Chin. J. Geolog. Hazard Control* vol. 16, no. 3, pp. 138–141, Mar. 2005.

[16] M. Liu, Y. He, J. Wang, H. P. Lee, and Y. Liang, "Hybrid intelligent algorithm and its application in geological hazard risk assessment," *Neurocomputing*, vol. 149, pp. 847–853, Feb. 2015.

[17] A. Malheiro, "Geological hazards in the azores archipelago: Volcanic terrain instability and human vulnerability," *J. Volcanology Geothermal Res.*, vol. 156, nos. 1–2, pp. 158–171, Aug. 2006.

[18] R. Sulpizio, G. Zanchetta, B. Caron, P. Dellino, D. Mele, B. Giaccio, D. Insinga, M. Paterne, G. Siani, A. Costa, G. Macedonio, and R. Santacroce, "Volcanic ash hazard in the central mediterranean assessed from geological data," *Bull. Volcanology*, vol. 76, no. 10, p. 866, Sep. 2014.

[19] R. Fell, K. K. S. Ho, S. Lacasse, and E. Leroi, "A framework for landslide risk assessment and management," in *Landslide Risk Management*. London, U.K.: Taylor & Francis, Jan. 2005, pp. 3–26.

[20] C. Z. Sheng, W. J. Gan, S. M. Liang, W. T. Chen, and G. R. Xiao, "Identification and elimination of non-tectonic crustal deformation caused by land water from GPS time series in the Westrern based on GRACE observations," *Chin. J. Geophys.*, vol. 57, no. 1, pp. 42–52, Jan. 2014.

[21] D. F. Argus, Y. Fu, and F. W. Landerer, "Seasonal variation in total water storage in California inferred from GPS observations of vertical land motion," *Geophys. Res. Lett.*, vol. 41, no. 6, pp. 1971–1980, Mar. 2014.

[22] T. van Dam, J. Wahr, and D. Lavallée, "A comparison of annual vertical crustal displacements from GPS and gravity recovery and climate experiment (GRACE) over Europe," *J. Geophys. Res.*, vol. 112, no. B3, Mar. 2007, Art. no. B03404.

[23] K. Terzaghi, "Mechanisms of landslides," Geol. Soc. Amer., Berkeley, CA, USA, Tech. Rep., Sep. 1950, pp. 83–123.

[24] S. A. Taqieddin, N. S. Abderahman, and M. Atallah, "Sinkhole hazards along the eastern dead sea shoreline area, jordan: A geological and geotechnical consideration," *Environ. Geol.*, vol. 39, no. 11, pp. 1237–1253, Oct. 2000.

[25] E. Nikolaeva, T. R. Walter, M. Shirzaei, and J. Zschau, "Landslide observation and volume estimation in central georgia based on L-band InSAR," *Natural Hazards Earth Syst. Sci.*, vol. 14, no. 3, pp. 675–688, Mar. 2014.

[26] R. Zhang, Z. Q. Jiang, C. L. Jiang, S. Y. Sun, and Q. Sun, "Study on foundation stability of surface buildings above mining Goaf in minefield of Hanqiao mine," *Coal Eng.*, vol. 4, pp. 61–63, Apr. 2011.

[27] L. Pfeifer-Meister and S. D. Bridgham, "Seasonal and spatial controls over nutrient cycling in a pacific northwest prairie," *Ecosystems*, vol. 10, no. 8, pp. 1250–1260, Nov. 2007.

[28] M. Métois, A. Socquet, C. Vigny, D. Carrizo, S. Peyrat, A. Delorme, E. Maureira, M.-C. Valderas-Bermejo, and I. Ortega, "Revisiting the north chile seismic gap segmentation using GPS-derived interseismic coupling," *Geophys. J. Int.*, vol. 194, no. 3, pp. 1283–1294, Jun. 2013.

[29] Y. S. Daniélyan and P. A. Yanitskii, "Stability of the interphase surface in the freezing of moist ground," *J. Eng. Phys.*, vol. 39, no. 1, pp. 781–785, Jul. 1980.

[30] C. Y. Zhang, T. Jiang, B. G. Ke, and W. Wang, "The analysis of height system definition and the high precision GNSS replacing leveling method," *Acta Geodaetica Et Cartographica Sinica*, vol. 8, pp. 11–17, Aug. 2017.
[31] P. Aleotti, "A warning system for rainfall-induced shallow failures," *Eng. Geol.*, vol. 73, nos. 3–4, pp. 247–265, Jun. 2004.
[32] R. L. Baum, J. A. Coe, J. W. Godt, E. L. Harp, M. E. Reid, W. Z. Savage, W. H. Schulz, D. L. Brien, A. F. Chleborad, J. P. McKenna, and J. A. Michael, "Regional landslide-hazard assessment for Seattle, Washington, USA," *Landslides*, vol. 2, no. 4, pp. 266–279, Nov. 2005.
[33] M. T. Brunetti, S. Peruccacci, M. Rossi, S. Luciani, D. Valigi, and F. Guzzetti, "Rainfall thresholds for the possible occurrence of landslides in italy," *Natural Hazards Earth Syst. Sci.*, vol. 10, no. 3, pp. 447–458, Mar. 2010.
[34] M. Calvello and L. Piciullo, "Assessing the performance of regional landslide early warning models: The EDuMaP method," *Natural Hazards Earth Syst. Sci.*, vol. 16, no. 1, pp. 103–122, Jan. 2016.
[35] P. Frattini, G. Crosta, and R. Sosio, "Approaches for defining thresholds and return periods for rainfall-triggered shallow landslides," *Hydrolog. Processes*, vol. 23, no. 10, pp. 1444–1460, May 2009.
[36] D. Salciarini, E. Volpe, S. A. Kelley, L. Brocca, S. Camici, G. Fanelli, and C. Tamagnini, "Modeling the effects induced by the expected climatic trends on landslide activity at large scale," *Procedia Eng.*, vol. 158, pp. 541–545, Jan. 2016, doi: 10.1016/j.proeng.2016.08.486.
[37] M. S. Rawat, V. Joshi, B. S. Rawat, and K. Kumar, "Landslide movement-monitoring using GPS technology: A case study of Bakthang landslide, Gangtok, East Sikkim, India," *J. Development Agricult. Econ.*, vol. 3, no. 5, pp. 194–200, Apr. 2011.
[38] Z. Feng, Bin. Li, C. Y. Zhao, L.Wang, and L. Wang, "Geological hazards monitoring and application in mountainous town of three gorges reservoir," *J. Geomech.*, vol. 22, no. 3, pp. 685–694, Mar. 2016.
[39] J. A. Gili, J. Corominas, and J. Rius, "Using global positioning system techniques in landslide monitoring," *Eng. Geol.*, vol. 55, no. 3, pp. 167–192, Feb. 2000.
[40] L. Cascini, "Applicability of landslide susceptibility and hazard zoning at different scales," *Eng. Geol.*, vol. 102, nos. 3–4, pp. 164–177, Dec. 2008.
[41] W. E. Farrell, "Deformation of the Earth by surface loads," *Rev. Geophys.*, vol. 10, no. 3, p. 761, 1972.
[42] W. Wei, D. Ya-Min, Z. Chuan-Yin, B. Li-Feng, L. Shi-Ming, H. Zhi-Tang, and Z. Zheng-Bo, "Monitoring of crustal deformation and gravity variations from terrestrial water loading in the Three Gorges region based on CORS network," *Chin. J. Geophys.*, vol. 60, no. 2, pp. 154–163, Mar. 2017.
[43] M. Dahl, B. Nilsson, J. H. Langhoff, and J. C. Refsgaard, "Review of classification systems and new multi-scale typology of groundwater–surface water interaction," *J. Hydrol.*, vol. 344, nos. 1–2, pp. 1–16, Sep. 2007.
[44] A. Lombard, D. Garcia, G. Ramillien, A. Cazenave, R. Biancale, J. M. Lemoine, F. Flechtner, R. Schmidt, and M. Ishii, "Estimation of steric sea level variations from combined GRACE and Jason-1 data," *Earth Planet. Sci. Lett.*, vol. 254, nos. 1–2, pp. 194–202, Feb. 2007.
[45] G. Blewitt and P. Clarke, "Inversion of Earth's changing shape to weigh sea level in static equilibrium with surface mass redistribution," *J. Geophys. Res.* vol. 108, p. 2311, Apr. 2003.
[46] R. Hoeben and P. A. Troch, "Assimilation of active microwave observation data for soil moisture profile estimation," *Water Resour. Res.*, vol. 36, no. 10, pp. 2805–2819, Oct. 2000.
[47] D. Dong, P. Fang, Y. Bock, M. K. Cheng, and S. Miyazaki, "Anatomy of apparent seasonal variations from GPS-derived site position time series," *J. Geophys. Res., Solid Earth*, vol. 107, no. B4, pp. ETG 9-1–ETG 9-16, Apr. 2002.
[48] J. A. R. Blais, D. A. Provins, and M. A. Soofi, "Spherical harmonic transforms for discrete multiresolution applications," *J. Supercomput.*, vol. 38, no. 2, pp. 173–187, Nov. 2006.
[49] Y. M. Dang, Q. Yang, and W. Wang, "Geodetic method and application for monitoring the stability of regional geological environment," *Acta Geologica et Cartographica Sinica*, vol. 46, no. 10, pp. 1336–1345, Jun. 2017.
[50] J. L. Davis, "Climate-driven deformation of the solid Earth from GRACE and GPS," *Geophys. Res. Lett.*, vol. 31, no. 24, 2004, Art. no. 3702004.
[51] C. Y. Zhang, A. Q. Li, Y. M. Dang, W. H. Mao, T. Jiang, W. Wang, and Q. Yang, "A method of tracking and monitoring of regional time-varying gravity field and ground stability based on CORS network," *Sci. Surv. Mapping*, vol. 44, no. 252, pp. 29–36, Jun. 2019.

PENGFEI XU received the M.Sc. degree in geomatics science and technology from the Shandong University of Technology, Zibo, China, in 2018. He is currently pursuing the Ph.D. degree in geodesy with the Shandong University of Science and Technology, Qingdao, China. His research interests include geodesy, geodynamics, geodetic data processing, load impact, applications of gravity recovery and climate experiment (GRACE), and monitoring of geological hazards.

AIQIN LI received the Ph.D. degree in photogrammetry and remote sensing from Wuhan University, Wuhan, China, in 2001. He is currently a Professor of engineering with the ZJ Academy of Surveying & Mapping, Zhejiang, China. His research interests include spatial geography big data, theory and application of geographic information, digital city, and data processing of remote sensing.

CHUANYIN ZHANG received the Ph.D. degree in geodesy from Wuhan University, Wuhan, China. He is currently a Professor with the Chinese Academy of Surveying and Mapping, Beijing, China. He is also an Adjunct Professor with the Shandong University of Science and Technology. He has presided over and completed many national scientific research projects, such as the Ministry of Science and Technology and the National Natural Science Foundation of China. He has published over 80 articles in geodesy and geodynamics. His research interests include load impact, earth gravity field, vertical geodetic datum, and monitoring of geological hazards.

YANG LIU received the M.Sc. degree in geomatics science and technology from the Shandong University of Science and Technology, Qingdao, China, in 2014, where he is currently pursuing the Ph.D. degree in geodesy. His research interests include marine geodesy, geodynamics, geodetic data processing, load impact, sea level anomaly, and monitoring of geological hazards.

WANQIU LI received the Ph.D. degree in geodesy from the Shandong University of Science and Technology, Qingdao, China, in 2019. She is currently a Lecturer with the School of Surveying and Geo-Informatics, Shandong Jianzhu University. Her research interests include load impact, earth gravity field, and applications of satellite gravity.